Available online at http://www.ifgdg.org

Int. J. Biol. Chem. Sci. 17(6): 2575-2594, October 2023

ISSN 1997-342X (Online), ISSN 1991-8631 (Print)

International Journal of Biological and Chemical Sciences

Original Paper http://ajol.info/index.php/ijbcs http://indexmedicus.afro.who.int

Absorbance enhancement of a treated Tanzanian kaolin for removal of synthetic dyes from contaminated water

Laurance ERASTO[1,2], Harieth HELLAR-KIHAMPA[1,3*] Quintino Alphonce MGANI[1] and Esther Hellen Jason LUGWISHA[1]

[1]*Chemistry Department, College of Natural and Applied Sciences, University of Dar es Salaam, P. O. Box 35061, Dar es Salaam, Tanzania.*
[2]*Government Chemist Laboratory Authority, P. O. Box 164, Dar es Salaam, Tanzania.*
[3]*Faculty of Science, Technology and Environmental Studies, The Open University of Tanzania, P. O. Box 23409, Dar es Salaam, Tanzania.*
[*]*Corresponding author; E-mail: hhellar@yahoo.co.uk; hariet.hellar@out.ac.tz*

Received: 31-08-2023 Accepted: 20-10-2023 Published: 31-10-2023

ABSTRACT

Kaolin possesses unique features suitable for removing pollutants from aqueous solutions, in this regard, improving its effectiveness as an adsorbent is important. This study focused on refining the absorbance efficiency of Pugu kaolin clay from Tanzania to enhance its utilization in removing textile dyes from contaminated water. The process involved acid-activation after calcination at 750°C. Characterization using X-ray Fluorescence (XRF), X-ray diffraction (XRD), Attenuated Total Reflectance-Fourier Transform Infrared Spectroscopy (ATR-FTIR) and Porosimeter techniques revealed the presence of kaolinite [$Al_2Si_2O_5(OH)_4$], silica (SiO_2) and microcline [$KAlSi_3O_8$] as the main phases. Acid treatment resulted in an increase in silica content from 44.18% to 58.81% due to the appearance of tridymite, while alumina decreased from 26.70% to 12.74% due to the removal of kaolinite. Surface area significantly expanded from 15.36 to 149.61 m^2/g as acid-soluble impurities were eliminated. Chemical composition was also altered, with a decrease in Fe_2O_3 and increase in other major oxides. The impact of acid activation on the adsorption capacity of the clay was investigated by studying various parameters such as contact time, temperature, adsorbent dose, initial pH and adsorbate concentration. Basic Blue 9 (BB9) and Direct Red 28 (DR28) dyes were used as model adsorbates. The results obtained at optimal conditions of 3 hours contact time, 27°C temperature, 0.9 g adsorbent dose, initial pH of 11 and initial adsorbate concentration of 90 mg/L, showed that acid modification of the clay increased its capacity to adsorb BB9 from 96.82% to 99.91%, and DR28 from 86.33% to 95.04%. These findings underscore the positive impact of modifying the raw clay, enhancing its suitability for dye removal applications.

Keywords: Batch adsorption technique; dye removal applications; clay modification; Tanzanian local kaolin.

INTRODUCTION

The utilization of kaolin clays as potential adsorbent materials in various environmental applications have been widely researched in numerous countries and areas e.g., the Botswana Lobatse clay (Sejie and Nadiye-Tabbiruka, 2016); the Brazilian kaolin (Caponi et al., 2017); the Moroccan Rhassoul

DOI: https://dx.doi.org/10.4314/ijbcs.v17i6.34

and Red clays (Bentahar et al., 2019); the Ethiopian clay (Aragaw and Angerasa, 2020; Mulushewa et al., 2021) and the Tanzanian Malangali kaolinite (Malima, 2021). One important application of clay adsorbents is the removal of synthetic dyes from contaminated waters (Mustapha et al., 2019; Chandan et al., 2021). Pollution of surface waters by synthetic dyes is one of the emerging issues of environmental concern. This is particularly due to the fact that there currently exist thousands of commercially available dyes with a wide range of uses in everyday human life. These include fabric colouring in textile industries, production of inks and artistic colours, in food production e.g., soft drinks, sauces and jellies and in cosmetic industries, e.g., hair dyes. This may cause significant amounts of dye residues to find their way to water sources during the course of their production and applications. Dye-containing effluents have the potential to cause adverse effects if not properly treated, including toxicity to human and aquatic biota, depletion of dissolved oxygen and reduction of the amount of light (Berradi et al., 2019). The concentration of some dyes at levels exceeding 1 mg/L in water may be visible to the naked eye enough to raise public concerns (Rahman et al., 2015). On the other hand, dyes are inherently designed to be stable to light, heat, and oxidizing agents (Avila et al., 2021), making their removal from water more complicated. When utilizing clays for dye-removal purposes, the efficiency of their absorbance properties is therefore important for realizing the desired outcome. Of recent, modification of clays to enhance their adsorption efficiency have received continuous attention Nwuzor et al., 2018; Gil et al., 2021). Some reported kaolin clay modifications methods include alkaline treatment (Zaini et al., 2021); surfactant modification (Mudzielwana et al., 2019); hybridization (He et al., 2019; Jawad and Abdulhameed, 2020); acid activation (Gao et al., 2016) and thermal treatment David et al. (2020). The essence of these modifications is to alter the vital clay properties that play important roles in their adsorption properties, such as surface area, ion exchange capacity, and chemical and mechanical stability (Li et al., 2016).

Tanzania is endowed with probably one of the largest kaolin deposits in the world, at Pugu, in Kisarawe District, Coast Region, southwest of Dar es Salaam city (UNEP, 2021). The Pugu kaolin clay has been widely investigated in relation to its applicability in various ways (Akwilapo and Wiik, 2004; Kimambo et al., 2014; Lugwisha and Siafu, 2014). However, its application as an adsorbent in the removal of dyes from polluted water has not been investigated. In this study, the raw Pugu kaolin clay (RPK) was first characterized to establish its chemical and mineralogical compositions, and its performance efficiency in removing textile dyes from contaminated water was tested using Basic Blue 9 (BB9) and Direct Red 28 (DR28) dyes as representative adsorbates. The raw clay was then modified through acid activation to obtain acid-activated Pugu kaolin clay (AAPK) with perceived improved quality. The main objective of the study was to investigate the effects of acid activation on the clay, focusing on the resulting changes in its mineralogical and chemical compositions, as well as the percentage enhancement of the adsorption efficiency after the modification. Further to that, a series of batch adsorption experiments were conducted using the two sample dyes to establish the optimum operating parameters for the dye's removal.

MATERIALS AND METHODS

Study site and preparation of the raw clay

The clay sample used in this study was obtained from the Pugu clay deposit in Kisarawe District, Coast Region, Tanzania, located at latitude and longitude 6° 52' 29" South and 39° 2' 48" East, respectively. The raw kaolin clay lumps were air dried, crushed, and ground with mortar and pestle, then sieved through a 300 µm sieve. The resulting fine powdery kaolin was then subjected to the quartering technique to obtain a representative sample. The resulting sample was mixed with distilled water and stirred for 4 hours, followed by the addition of a small amount of hydrogen peroxide (H_2O_2). The mixture was left to settle

overnight to allow the dissolution of impurities, followed by decantation and vacuum filtration. Thereafter, water was re-added to the kaolin residue and allowed to settle again for 3 hours, which was followed by decantation and filtration to remove more impurities and hydrogen peroxide. This process was repeated four times from which the final obtained kaolin residue was dried in a Genlab oven at 100ºC for 12 hours to obtain the RPK, which was stored in an airtight plastic container for later instrumental characterization, preparation of the acid-activated clay and running of adsorption studies.

Chemicals, reagents, and equipment

All the chemicals used in this study were of analytical grade obtained from certified chemical suppliers. The chemicals included sodium hydroxide (NaOH) of assay 99% obtained from Blulux Laboratories (P) Ltd; hydrochloric acid (HCl) of assay 37% and hydrogen peroxide (H_2O_2) of assay 30% obtained from Scharlau Chemie SA, Spain; sulfuric acid (H_2SO_4) of assay 98% obtained from Fisher Scientific, UK; barium chloride ($BaCl_2$) of assay 98% obtained from J.T. Baker Chemical Company, U.S.A; trihydrated basic blue dye (BB9) ($C_{16}H_{18}ClN_3S.3H_2O$) of assay 85% obtained from UNI-CHEMI; direct red dye (DR28) ($C_{32}H_{12}N_2Na_2O_6S_2$) of assay 95% obtained from Loba Chemie PVT Ltd and distilled water prepared at the Chemistry Department, University of Dar es Salaam. The instruments used in this study included alpha ATR-FTIR spectrometer (model: Bruker Optic GmbH 2011, U.S.A), X-ray powder diffractometer (model: BTX 231, Inxitu inc., U.S.A), Nova 1200e Porosimeter (surface area, pore volume and pore diameter analyzer, model: N12-28E, Quantachrome Corporation, Japan) and UV-Vis spectrophotometer (Analytikjena SPECORD 210 PLUS – 223F1376), obtained at the Department of Geosciences, School of Mines and Geosciences, University of Dar es Salaam and X-Ray Fluorescence spectrometer (model: S8 Tiger-SN. 206548, Bruker AXS company, Germany) obtained at the African Minerals and Geosciences Centre, Kunduchi, Dar es Salaam.

Acid activation treatment of the raw clay

The RPK sample was first calcined at a temperature of 750ºC in a muffle furnace for 7 hours, then cooled to room temperature in a desiccator, forming calcined Pugu kaolin (CPK) clay. The obtained CPK was further chemically beneficiated by acid leaching. In the process, five CPK samples, each weighing 50 g were acid leached with 500 mL of 0.1, 0.2, 0.4, 0.8, and 1.2 M sulfuric acid (H_2SO_4) solution, respectively. The process was carried out at 100ºC under reflux conditions with constant stirring for 3 hours. The resulting suspension was washed through the addition of distilled water, followed by vacuum filtration to remove excess sulfuric acid. The filtrate obtained was treated with a pre-prepared barium ion (Ba^{2+}) solution to test for the presence of sulfate ion (SO_4^{2-}), whereby barium sulfate ($BaSO_4$) precipitates were formed. The washing process was repeated several times to the point that filtered filtrate did not form precipitates of $BaSO_4$ with barium (Ba^{2+}) solution. This point signified a neutral point by which the obtained residue was free of sulfuric acid used during the leaching process. The resulting residues were then dried in an oven at 100ºC for 12 hours, cooled to room temperature for 3 hours in a desiccator, ground, and re-sieved through a 300 µm sieve to obtain the AAPK samples. The adsorbent samples were kept in separate airtight plastic containers for further use in the adsorption studies and determination of the optimal activation concentration of sulfuric acid that would give the AAPK adsorbent the maximum adsorption efficiency.

Preparation of the adsorbates

The standard stock BB9 solution of 1 g/L concentration was prepared by dissolving 0.69 g BB9 powder in distilled water to make 0.5 L of a deep blue solution. The solid powder dye was first dissolved in a small amount of distilled water, followed by the addition of more water to the mark of the 500 mL flat-bottomed volumetric flask, then thoroughly mixed. The standard stock DR28 solution of 1 g/L concentration was similarly prepared by dissolving 0.53 g of DR28 powder in 0.5 L of

distilled water to form a deep red solution. The resulting two adsorbate solutions were then stored away from light in the plastic bottles for preparation of the BB9 and DR28 adsorbate working solutions that were used in the adsorption studies. These were prepared in the concentration range of 0.1 – 100 mg/L by diluting respective BB9 and DR28 stock solutions based on the dilution law equation:

$$C_i V_i = C_d V_d \quad (1)$$

whereby a given amount of distilled water was added to an initial volume V_i with concentration C_i of the stock solution to make a new volume V_d of dilute working solution with desired concentration C_d.

Characterization of the adsorbents

Instrumental characterizations were performed to identify functional groups, mineralogical compositions, chemical composition, and porosity of the raw as well as the acid-activated clay samples. Determination of the available functional groups was performed by an ATR-FTIR spectrometer connected to a computer for data manipulation. Small amounts of fine powder samples were pressed against a prism with a high refractive index, from which the internally reflected infra-red radiations within the prism gave rise to the respective IR spectra in the range of 400 – 4000 cm^{-1} wavenumbers. The mineralogical compositions were determined by an X-Ray powder diffractometer (model: BTX 231) connected to a computer with installed XPowder interface software. About 20 mg of homogeneous fine powder of each of the two clay samples previously prepared, were placed into the sample cell. The samples were then bombarded with generated X-rays by the instrument under operating conditions of temperature of -45°C, voltage of 30.03 kV, and current of 0.30 mA; from which respective XRD patterns for RPK and AAPK were recorded. The d-spacing values for different identified mineral phases for each sample were determined within the position range between 5-55° 2θ. The elemental compositions, defined by the major oxides of the RPK and the AAK, were determined by an S8 Tiger XRF spectrometer with a power of 5.2 kVA. About 10 g of fine powder of each sample was mixed with a few drops of boric acid, a binding agent, then compressed into circular pellets of 34 mm diameter. The sample pellets were separately introduced into the sample tray of the instrument for analysis of both quantitative and qualitative elemental composition of the samples.

Three physical parameters of surface area, pore volume, and pore diameter of the RPK and AAPK samples were analyzed by a Nova 1200e Porosimeter using a nitrogen adsorption-desorption technique at 77.35 K and relative pressure in the range of 0.05 and 0.35. The porosimeter was connected to a computer with NovaWin software installed in it for the measurement of surface area, pore volume, and pore diameter. About 0.1 g of each RPK and AAPK fine powdery sample were first degassed at 160°C to remove previously physisorbed contaminants. Then each sample was allowed to interact with liquid nitrogen for adsorption-desorption analysis, from which respective the surface area, pore volume, and diameter of the samples were obtained.

Batch adsorption experiments

Pre-adsorption studies

Adsorption studies were preceded by the determination of optimal wavelengths for BB9 and DR28, preparation of calibration curves for respective adsorbates as well as determination of the pH at the Zero Point of Charge (pH_{ZPC}). Maximal absorbances for BB9 and DR28 adsorbates were measured by Analytikjena SPECORD 210 PLUS UV-Vis spectrophotometer. About 3 mL of standard solutions (2.50, 3.00, and 3.50 mg/L of BB9; and 11.50, 15.50, and 18.00 mg/L of DR28) were placed in the cuvette and then introduced into the instrument for determination of maximum absorbances corresponding to the respective optimal wavelengths for BB9 and DR28. The optimal wavelengths were determined through spectral scan mode within the visible region (350 – 800 nm). These optimal wavelengths were then used in the measurements of the maximum absorbances in the determination of the BB9 and DR28 calibration curves as well as various

supernatants obtained in the course of adsorption studies. Several standard solutions of BB9 in the range of 0.1 - 6.0 mg/L at pH of 6.81 and temperature of 27°C were prepared, followed by measurements of respective maximum absorbance by UV-Vis spectrophotometer at the predetermined optimal wavelength of 665 nm. In the same way, standard solutions of DR28 in the range of 0.8 - 30 mg/L were prepared, followed by measurements of respective maximum absorbances at the predetermined optimal wavelength of 500 nm. In each case, a linear plot of absorbance against concentration were obtained based on Beer-Lambert's law equation:

$$A = \varepsilon lc \quad (2)$$

Where: A = absorbance; l = path length (cm); c = concentration of solution (mol/L) and ε = Molar absorptivity (L mol^{-1} cm^{-1}). The plots were used to determine the respective free or equilibrium concentration of each adsorbate dye available in the adsorbent-adsorbate system after a given contact time. To determine the pH at the Zero Point of Charge (pH_{ZPC}), ten samples of RPK of 0.5 g each and particle size of 300 µm, were mixed with 0.05 L of distilled water of known initial pH in the range of 2 - 11. Adjustment of pH was attained by the addition of a few drops of either dilute HCl or NaOH. The systems (water-RPK mixture) was shaken for 12 h at 27ºC to the attain final equilibrium pH. The initial and final pH of each system was measured by a digital pH meter. Thereafter determination of the pH_{ZPC} was made from the plot of final pH against initial pH.

Adsorption studies

In this experiment, the effects of temperature, adsorbent dose, initial pH of adsorbate solution, contact time, and initial adsorbate concentration on adsorption efficiency of RPK and AAPK adsorbents were investigated. The experiments were preceded by the determination of the AAPK adsorbent corresponding to the optimal activation concentration of sulfuric acid, which exhibited maximum adsorption efficiency for both BB9 and DR28 adsorbates. In determining the optimal activation concentration of sulfuric acid, a solution of 0.05 L with 30 mg/L of BB9 adsorbate was added to six adsorbent samples, each weighing 0.5 g and particle size of 300 µm. Out of these adsorbents, five samples were of AAPK leached with 0.1, 0.2, 0.4, 0.8, and 1.2 M H_2SO_4 and one was of RPK as a reference sample. The pH of each system was then adjusted to 6.80 by the addition of a few drops of either HCl or NaOH dilute solution. Similarly, DR28-adsorbent systems were prepared. This pair of systems were then shaken at 26.5ºC for 3 hours. Thereafter, each system was centrifuged for 15 min at 4000 rpm to obtain respective supernatants for determination of the free concentration of BB9 and DR28, and the adsorption efficiency of each adsorbent. This data was used in the determination of AAPK adsorbent corresponding to the optimal activation concentration of sulfuric acid that gave maximum adsorption efficiency. The respective AAPK with maximum adsorption efficiency was used for further adsorption studies. To determine the free concentration for each adsorbate, about 3 mL of each supernatant dye solution obtained from adsorbate-adsorbent systems were placed in a cuvette for the measurement of absorbances by UV-Vis spectrophotometer at the pre-determined optimal wavelengths of $\lambda = 665$ nm and 500 nm for BB9 and DR28 solutions, respectively. These absorbances were then converted to corresponding equilibrium concentrations from predetermined BB9 and DR28 calibration curves.

Determination of the adsorption phenomenon

Adsorption isotherms were used to describe the adsorption equilibrium attained between adsorbent and adsorbate. Such equilibrium is essential in understanding the adsorption mechanism as well as the nature of adsorbent, adsorbate, and respective intermolecular forces (Sharma, 2015). They were also used to determine the thermodynamic data that play a central role in determining the spontaneity, viability, and favorability of the adsorption phenomenon. In this study, the Langmuir and Freundlich isotherms were used to examine the nature of the adsorption process between the BB9 and

DR28 adsorbates and the RPK and AAPK adsorbents.

The Langmuir adsorption isotherm (LAI) model characterizes ideal monolayer homogeneous adsorption, in which all adsorbent's adsorptive sites have equal energy and are equally available. In addition, it defines adsorption with neither interaction between adsorbed molecules nor transmigration of adsorbate molecules into the adsorbent surface. The linear form of the isotherm can be explained by the equation (Liu et al., 2019):

$$\frac{c_e}{q_e} = \frac{1}{bq_m} + \frac{c_e}{q_m} \quad (3)$$

Where: b = Langmuir constant (L mg $^{-1}$) which is related to adsorption energy, q_e = quantity of adsorbate adsorbed per unit adsorbent mass (mg/g), c_e = free or equilibrium concentration of adsorbate (mg/L), q_m = maximum adsorbent adsorption capacity (mg/g).

The Freundlich adsorption isotherm (FAI) describes non-ideal adsorption onto heterogeneous adsorbent surfaces, with the assumption that adsorbate concentration is directly related to the amount of adsorbate adsorbed. It is described by the equation (Singh, 2016):

$$lnq_e = lnK_f + \left(1/n\right) lnc_e \quad (4)$$

Where: q_e = amount of adsorbate adsorbed per unit mass of adsorbent at equilibrium (mg/g); c_e = free or equilibrium concentration of the adsorbate dye (mg/L); *1/n* = measure of adsorption intensity and K_f = Freundlich constant that measure adsorption capacity.

RESULTS

Characterization of the raw and acid-activated clays

Functional Groups

The ATR-FTIR absorption bands [Wavenumber (cm^{-1})] for RPK and AAPK adsorbents are presented in Figure 1(a) and (b). The figure shows that RPK displayed absorption peaks at 788.67 cm^{-1} (stretching vibration) and 752.92 cm^{-1} (bending vibration), characteristic of pure kaolinite. Additionally, the sharp peaks at 3687.28 cm^{-1} and 3619.17 cm^{-1}, denoting stretching vibrations, confirmed the presence of crystalline kaolinite in RPK. Other peaks at 688.06, 533.44, and 462.37 cm^{-1} (stretching vibrations) suggested the availability of kaolinite.

In contrast, AAPK exhibited a distinct ATR-FTIR spectrum, with reduced peak intensities and shifted bands. Acid activation transformed the sharp stretching vibration bands at 3687.24 cm^{-1} and 3619.38 cm^{-1} into a broad peak at 3372.92 cm^{-1}. Other shifts in peak positions included the bending vibration from 752.92 cm^{-1} to 724.56 cm^{-1} and stretching vibrations from 688.06 cm^{-1} to 645.75 cm^{-1}. The changes suggested significant structural alterations in the formation of AAPK, including the presence of amorphous silica. Notably, the appearance of a new peak at 1076.11 cm^{-1} (stretching vibration) further supported the presence of amorphous silica in AAPK. Furthermore, there was observed a transformation of a sharp peak at 533.44 cm^{-1} to a broad peak at 581.53 cm^{-1} (stretching vibrations) with significantly reduced peak intensity reinforced the notion of structural changes in RPK upon acid activation.

The AAPK adsorbent exhibited an ATR-FTIR spectrum which is different from that of RPK, where the peak intensities had been reduced while some bands had shifted. Figure 1 also shows that upon acid activation of the raw clay, the 3687.24 and 3619.38cm^{-1} (stretching vibrations) bands were transformed into a very broad peak and shifted to 3372.92 (stretching vibration); while the peak at 752.92 cm^{-1} shifted to 724.56 cm^{-1} (bending vibration), and that at 688.06 shifted to 645.75 cm^{-1} (stretching vibrations). These changes suggested structural changes of the RPK upon calcination followed by acid leaching in the formation of AAPK. Structural changes were further described by the disappearance of the 426.80 (bending), 911.73, and 1004.86 cm^{-1} (stretching vibrations) peaks as well as the appearance of the new peak at 1076.11 cm^{-1}(stretching vibration).

Figure 2 compares the ATR-FTIR spectra before and after adsorption. It indicates that almost all absorption bands remained the same but with reduced intensities after adsorption, implying that the physisorption between RPK and AAPK adsorbents and

adsorbates (BB9 and DR28) predominated over chemisorption. The decreased peak intensities of RPK and AAPK suggested that exposure of the respective adsorbent functional groups as a result of BB9 and DR28 adsorption were reduced. Furthermore, in all two cases, peaks corresponding to DR28 adsorption are much reduced than the peaks for BB9 adsorption.

Mineralogical composition

The X-ray diffraction (XRD) analysis of the two clays provided insights into the mineralogical composition of the clay before and after treatment. Figure 3 compares the XRD patterns of the raw (RPK) and the treated (AAPK) clays.

Figure 3(a) indicates that the XRD pattern of the RPK revealed the presence of three phases: i.e., kaolinite [$Al_2Si_2O_5(OH)_4$], quartz [SiO_2], and potassium feldspar or microcline [$KAlSi_3O_8$] as impurities in the kaolin sample. Major peaks corresponding to kaolinite had reflections at 2θ values of 14.40°, 23.5°, 29°, and 26.90°, with d values of 7.16, 4.35, 3.58, and 3.84 Å, respectively. These results indicated the presence of crystalline kaolinite with coarser grains in the RPK sample. The identification of microcline and quartz was based on their respective reflection peaks.

In contrast, the XRD pattern in Figure 3(b) revealed the presence of microcline, two polymorphs of silica (quartz and tridymite), and the absence of the kaolinite phase. Tridymite was identified with reflection peaks at d values of 4.10 and 3.82 Å, at 2θ positions of 25° and 27°. This shift towards increased silica content in AAPK was attributed to the calcination of kaolin at 750°C. Both quartz and microcline maintained their prominent d values, indicating that acid activation did not affect these phases. The disappearance of kaolinite peaks and the presence of tridymite suggested that calcination and acid leaching caused structural changes in raw kaolin.

The XRD pattern of AAPK (Figure 3b) indicates the presence of phases of microcline and two polymorphs of silica (quartz and tridymite) and the disappearance of the kaolinite phase. The identification of the microcline phase was based on the reflection giving several peaks, including major peaks defined by d values of 3.25 and 3.48 Å approximately to 2θ = 32° and 30°, respectively. Identification of quartz, a polymorph of silica phase in RPK sample was based on the presence of prominent reflection peak of d value corresponding to 3.35 and 4.2 Å at position approximately to 2θ = 31° and 24.5°, respectively. Tridymite was identified with reflection peaks at d values of 4.10, 3.82 Å approximately to a position of 25° and 27° 2θ, respectively. The presence of tridymite silica might be the result of the calcination reaction of the kaolin clay at 750°C which accounts for increased silica content in the AAPK sample as it has been observed from XRF analysis in this study. Microcline and quartz maintained their prominent d values of 3.25 and 3.48 Å approximately to 32° and 30° 2θ, respectively, for microcline. For quartz, the d values were 3.35 and 4.20 Å approximately to 31° and 24.5° 2θ. Such observation implies that quartz and microcline were not affected by acid activation.

Chemical composition

The results from the XRF analysis of chemical composition of the raw and the treated clays are summarized in Table 1. The data, which shows the composition of nine major oxides, revealed some changes after acid activation. The results show that six of the oxides i.e., SiO_2, CaO, K_2O, Na_2O, MnO, and P_2O_5 increased after acid activation by various degrees, while three of the oxides decreased.

There was an increase in the silica content from 44.18% to 58,81% after acid activation, which corresponds to the appearance of the tridymite phase. while the decrease in the alumina content from 26.70% to 12.74% corresponds to the disappearance of the kaolinite phase, as supported by the XRD results. Acid leaching was responsible for the dissolution of dialuminium silicate as per the chemical equation: $Al_2Si_2O_{7(s)} + 3H_2SO_{4(aq)} \rightarrow Al_2(SO_4)_{3(s)} + 2SiO_2(s) + 3H_2O_{(l)}$ leading to the observed changes in alumina content.

Physical parameters

The results from the porosimeter characterization demonstrated a substantial

change in specific surface area, pore volume, and pore diameter for the acid-activated clay (AAPK) compared to the raw clay (RPK). The calcination at 750°C followed by acid leaching caused the transformation of the kaolin into porous amorphous metakaolin characterized with increased surface area from 15.36 m^2/g to 149.61 m^2/g; decreased pore volumes from 0.033 cm^3/g to 0.026 cm^3/g; and increased pore diameters from 3.049 nm to 28.200 nm, for the raw and acid-activated clays, respectively. The increase in specific surface area indicated the removal of unwanted impurities and the transformation of kaolin into a more porous structure. The aggregation of fine particles likely accounted for the decreased pore volume of AAPK relative to RPK. Additionally, the significant increase in pore diameter for AAPK further indicated substantial modification to its properties.

Conditions for optimal adsorption efficiency

Concentration of sulfuric acid

Figure 4 compares the adsorption efficiencies of the modified clay after leaching with varied concentrations of H_2SO_4, using the two sample dyes, i.e., BB9 and DR28. It shows that the concentration of 0.2 M H_2SO_4 gave the highest adsorption of 96.96% and 93.55% for BB9 and DR28, respectively compared to that of the raw clay, which were 75.02% for BB9 and 34.16% for DR28. Activation with 0.2 M sulfuric acid gave the maximum increment in surface area to 149.61 m^2/g. These results indicate that 0.2 M can be regarded as the optimal activation concentration of H_2SO_4.

Operational Parameters

Temperature

Table 2 summarizes the results of the effect of temperature on the adsorption efficiency of adsorbents. The adsorption efficiency and quantity adsorbed per unit mass of adsorbent for BB9 and DR28 decreased as the temperature was raised from 27 to 90°C in the order of RPK < AAPK.

The data in Table 2 show that BB9 was adsorbed more with adsorption efficiency ranging from 81.45 to 61.58% for RPK and 96.62% to 81.23% for AAPK; while for DR28, the adsorption efficiency decreased from 51.71% to 38.63% for RPK and 62.45% to 44.75% for AAPK. The observed trend implies that the adsorption processes were more favorable at low temperatures and exothermic. The exothermic nature of the adsorption process is supported by the negative values of the enthalpy change.

Adsorbent dose

Table 3 summarizes the effect of the adsorbent dose on the adsorption of the two dyes. It shows that the adsorption efficiency of adsorbents (A_e) increased and the quantity of adsorbate adsorbed per unit mass of adsorbent (q_e) decreased as the adsorbent dose increased. The data in Table 3 show the adsorption efficiency of BB9 increased from 40.82% to 96.82% for RPK and from 69.54% to 99.74% for AAPK; whereas that of DR28 increased from 25.62% to 46.11% for RPK and 31.82% to 82.08% for AAPK.

Initial pH

Figure 5 summarizes the results of the effect of initial pH on the adsorption efficiency of the two dyes. As the initial pH increased from 3, 5, 7, 9 to 11, the adsorption efficiency of BB9 increased from 68.71% to 94.73% for RPK and 94.13% to 98.85% for the AAPK at a pH value of 11, whereas for the DR28 it increased to the optimal adsorption of 86.33% for RPK and 94.03% for AAPK at pH value of 5, then decreased to the value of 56.86% for RPK, 63.44% and 67.83% for AAPK at pH value of 11.

Contact time

Table 3 summarizes the results of the variation of the adsorption efficiency of both BB9 and DR28 with varying contact time from 0, 20, 60, 100, 140 to 180 minutes.

The data in Table 4 show that the adsorption efficiency of both BB9 and DR28 increased with contact, however, in comparing the two dyes, the BB9 was adsorbed more compared to DR28. This indicates the importance of the dye type as well. The adsorption rate was found to be faster in the first 20 min of contact time, from which the adsorption efficiency of BB9 increased to 83.59% and 99.25% for RPK and AAPK, respectively, while for DR28, the observed adsorption efficiencies were 41.76% and

49.43% for RPK and AAPK respectively. Thereafter percent color removal increased slowly to about equilibrium within contact time of 180 min. The maximum adsorptions were found to be 91.45% and 99.91% BB9 for RPK and AAPK respectively; while for DR28 observed optimal adsorption were 50.06% and 59.36% for RPK and AAPK respectively. The higher adsorption rate in the first few minutes of contact time accounts for the availability of enough free adsorptive sites as well as the surface area of the adsorbents. Later on, the number of free adsorptive sites and surface area decreased with increased contact time accounting for the observed slower adsorption rate. The attachment of adsorbate molecules onto the surface of the adsorbent accounts for decreased surface area as well as adsorptive sites available for further adsorption.

Initial concentration

The variation of the quantity of adsorbate adsorbed (q_e) with increased initial adsorbate concentration from 30, 45, 60, 75 to 90 mg/L showed that the activated clay AAPK achieved the highest adsorption capacity with optimal q_e of 6.429 and 8.634 mg/g respectively of BB9, and 4.232 and 6.917 mg/g of DR28 at an initial concentration of 90 mg/L. Increasing adsorbate concentration accounts for increased adsorbate molecules resulting in increased amount adsorbed per unit mass of adsorbent.

Adsorption Isotherms

The Langmuir and Freundlich adsorption isotherms for the two systems are presented in Figure 6. The Langmuir isotherms are linear with respective correlation coefficient (R^2) values of 0.983 and 0.975 for the RPK-BB9 and the AAPK-BB9 systems respectively, and 0.982 and 0.989 for the RPK-DR28 and the AAPK-DR28 systems respectively.

The obtained R^2 values that are close to unit, together with the obtained values of separation factor S_f that ranged between 0 and 1 ($0 < S_f < 1$) suggest favourable monolayer adsorption. However, the smaller value of S_f implies strong interaction between adsorbate and adsorbents hence it likely indicates less reversibility of the adsorption process. Further analysis of the S_f indicated that BB9 bound a bit stronger to the adsorbents DR28 in the AAPK than the RPK.

The Freundlich adsorption isotherms for the two dyes are linear with correlation coefficient values (R^2) of 0.906 and 0.924 for the RPK-DR28 and AAPK-DR28 adsorption systems respectively, while those for the RPK-BB9 and AAPK-BB9 systems corresponded to coefficient values of 0.900 and 0.990, respectively. The R^2 values that are approaching unit, together with the obtained values of adsorption intensity (n) in the range of 2-10 suggest favourable and multilayer adsorption of adsorbates onto a heterogeneous adsorbent surface.

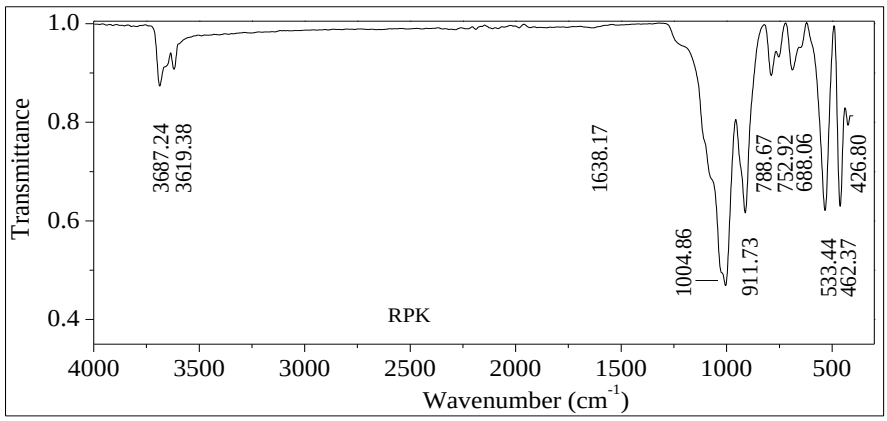

(**a**)

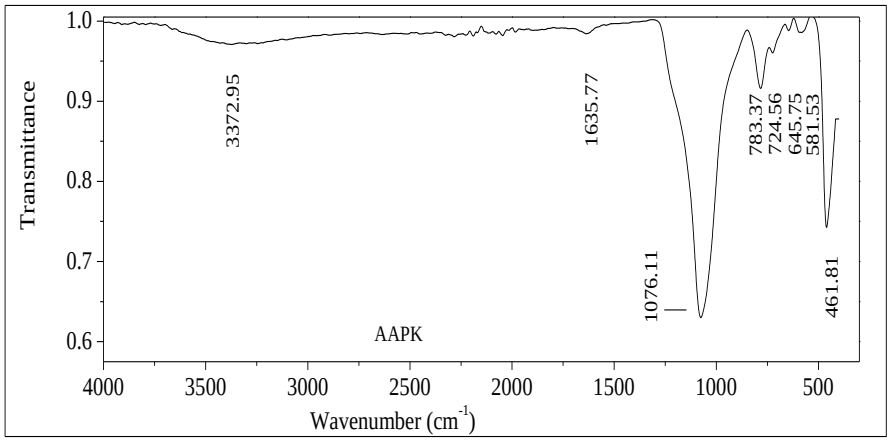

(**b**)

Figure 1: ATR-FTIR Spectra of RPK (a) and AAPK (b) showing the different absorption bands before and after treatment.

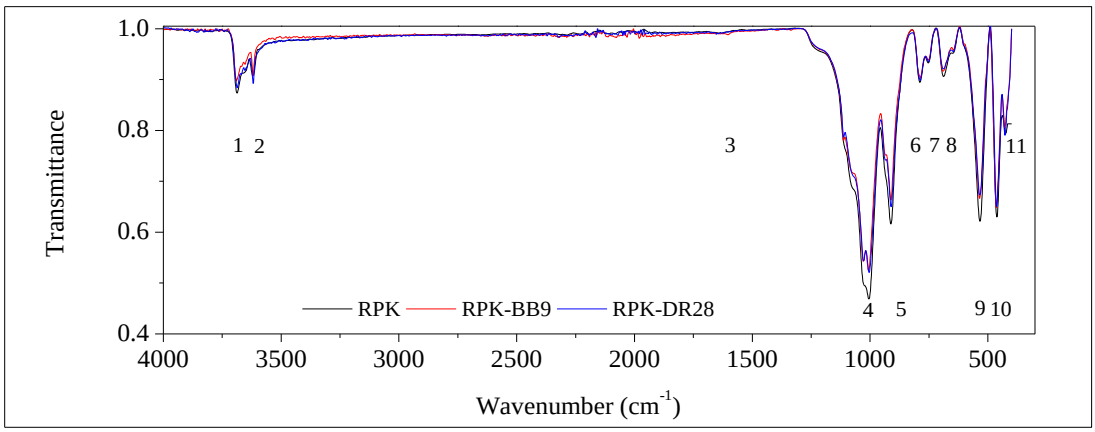

(**a**)

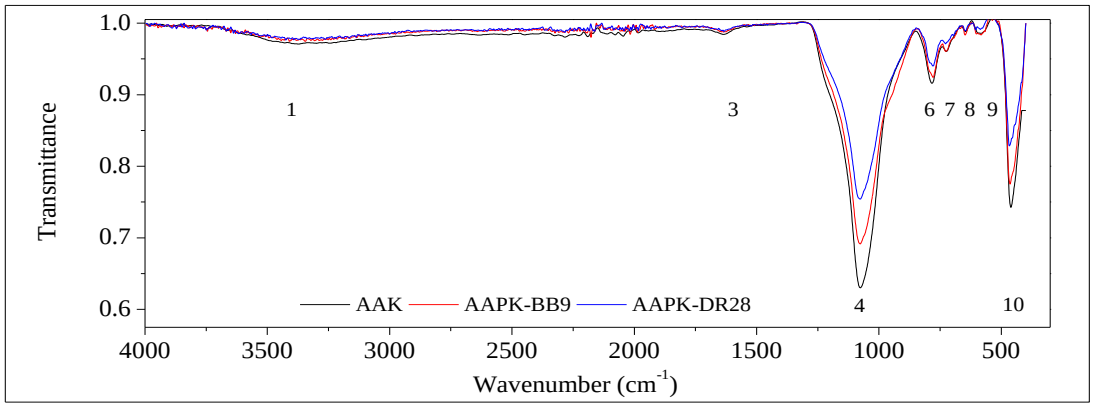

(**b**)

Figure 2: ATR-FTIR Spectra of RPK (a) and AAPK (b) showing the different adsorption bands before and after adsorption of the two dyes.

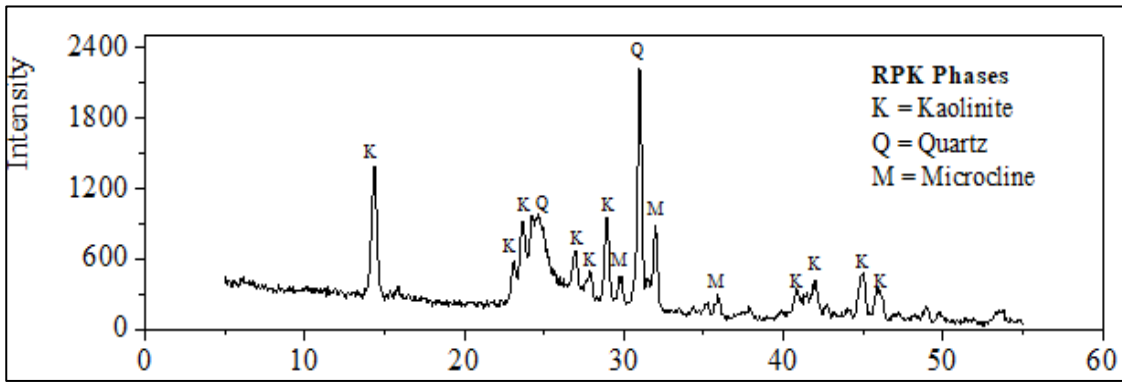

(**a**)

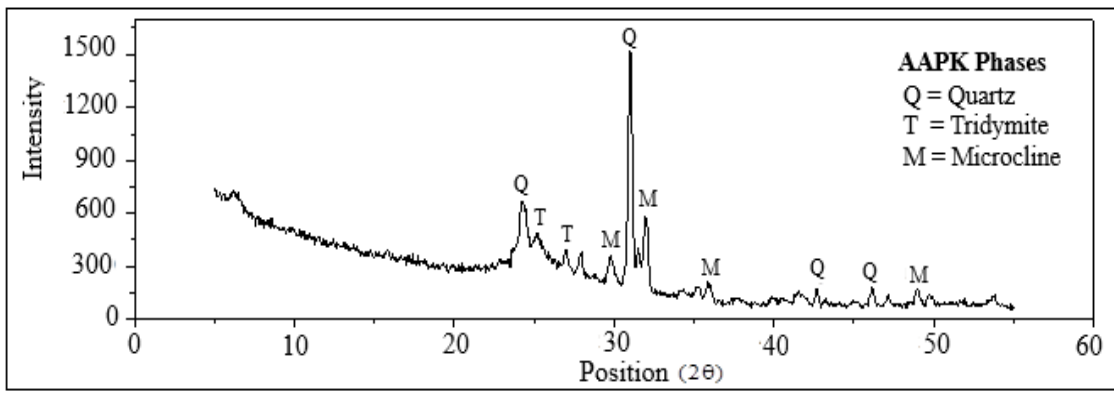

(**b**)

Figure 3: XRD patterns for RPK (a) and AAPK (b) showing the different mineralogical phases before and after treatment.

Table 1: Chemical compositions of the raw (RPK) and acid-activated (AAPK) clays.

Constituent	RPK Composition (%)	AAPK Composition (%)
SiO_2	44.18	58.81
Al_2O_3	26.70	12.74
Fe_2O_3	1.78	0.82
CaO	13.01	14.53
MgO	0.54	0.12
K_2O	1.73	1.87
Na_2O	0.04	0.07
MnO	0.02	0.05
P_2O_5	0.06	0.08
LOI	11.9	10.88

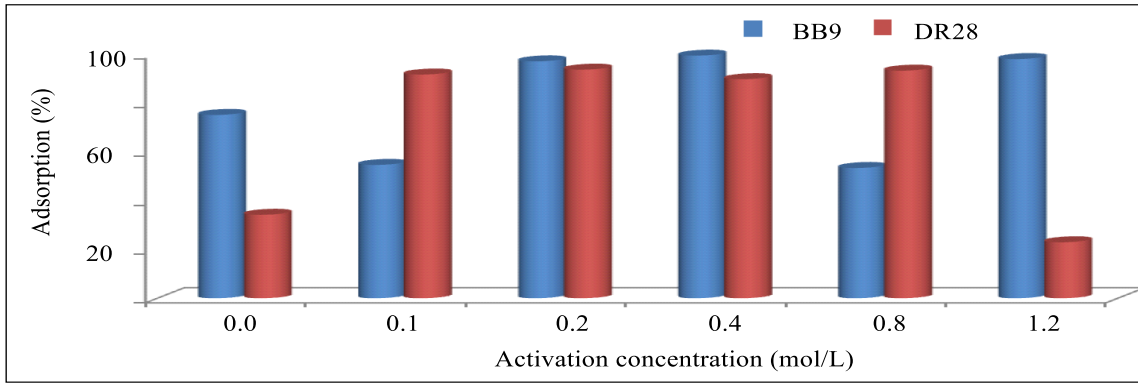

Figure 4: Adsorption efficiency of the modified clay for the two dyes at different H_2SO_4 activation concentrations.

Table 2: Effect of temperature on adsorption of BB9 and DR28.

Adsorbent	Temp (°C)	DR28			BB9		
		c_e (mg/L)	A_e (%)	q_e (mg/g)	c_e (mg/L)	A_e (%)	q_e (mg/g)
RPK	27	14.488	51.71	1.551	5.566	81.45	2.443
	43	15.068	49.77	1.493	7.963	73.46	2.204
	56	16.347	45.51	1.365	8.241	72.53	2.176
	76	17.883	40.39	1.212	9.995	66.68	2.000
	90	18.412	38.63	1.159	11.527	61.58	1.847
AAPK	27	11.264	62.45	1.874	1.014	96.62	2.899
	43	11.369	62.10	1.863	1.400	95.33	2.860
	56	12.492	58.36	1.751	2.128	92.91	2.787
	76	13.850	53.83	1.615	4.070	86.43	2.593
	90	16.575	44.75	1.343	5.630	81.23	2.437

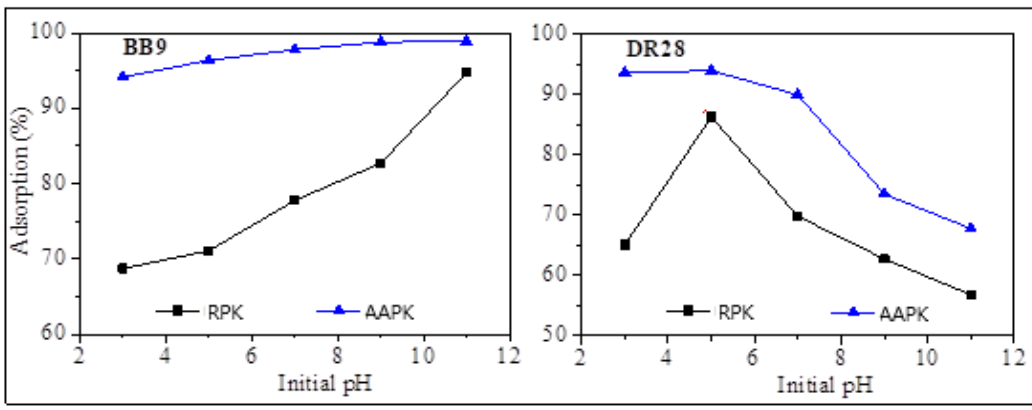

Figure 5: The effect of initial solution pH on adsorption of BB9 and DR28.

Table 3: The effect of adsorbent dose on BB9 and DR28 Adsorption.

Adsorbent	Dose (g)	BB9			DR28		
		c_e (mg/L)	A_e (%)	q_e (mg/g)	c_e (mg/L)	A_e (%)	q_e (mg/g)
RPK	0.1	17.755	40.82	6.123	22.315	25.62	3.843
	0.3	10.590	64.70	3.235	20.346	32.18	1.609
	0.5	4.801	84.00	2.520	18.711	37.63	1.129
	0.7	2.209	92.64	1.985	18.194	39.35	0.843
	0.9	0.955	96.82	1.614	16.167	46.11	0.768
AAPK	0.1	9.137	69.54	10.431	20.455	31.82	4.772
	0.3	1.846	93.85	4.692	17.003	43.32	2.166
	0.5	0.971	96.76	2.903	12.266	59.11	1.773
	0.7	0.338	98.87	2.119	10.156	66.15	1.417
	0.9	0.077	99.74	1.662	5.376	82.08	1.368

Table 4: Effect of the contact time on BB9 and DR28 Adsorption.

Adsorbent	Time (min)	BB9			DR28		
		c_e (mg/L)	A_e (%)	q_e (mg/g)	c_e (mg/L)	A_e (%)	q_e(mg/g)
RPK	20	4.922	83.60	2.508	17.473	41.76	1.253
	60	3.221	89.26	2.678	15.565	48.12	1.444
	100	3.072	89.76	2.693	15.507	48.31	1.449
	140	2.599	91.34	2.740	15.059	49.80	1.494
	180	2.566	91.45	2.743	14.983	50.06	1.502
AAPK	20	0.225	99.25	2.977	15.171	49.43	1.483
	60	0.097	99.68	2.990	13.492	55.025	1.651
	100	0.056	99.81	2.994	13.247	55.84	1.675
	140	0.051	99.83	2.995	12.725	57.58	1.727
	180	0.028	99.91	2.997	12.193	59.36	1.781

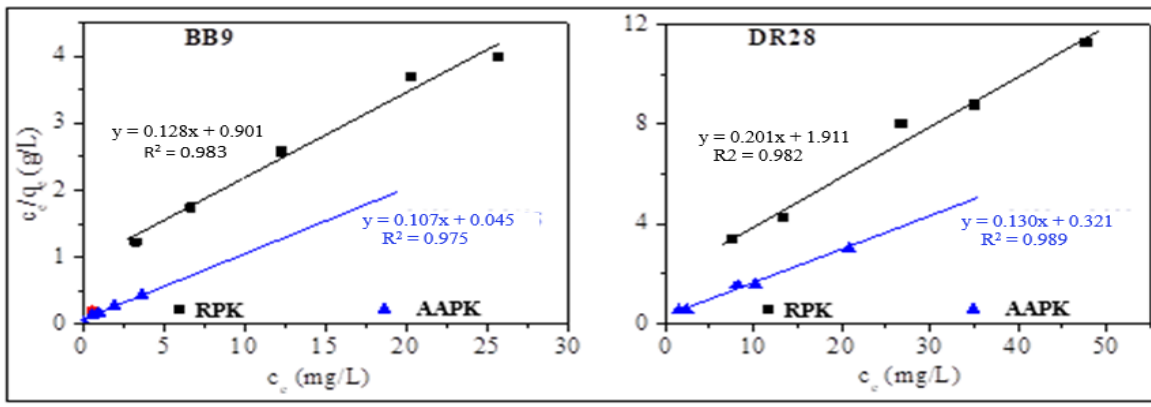

(a)

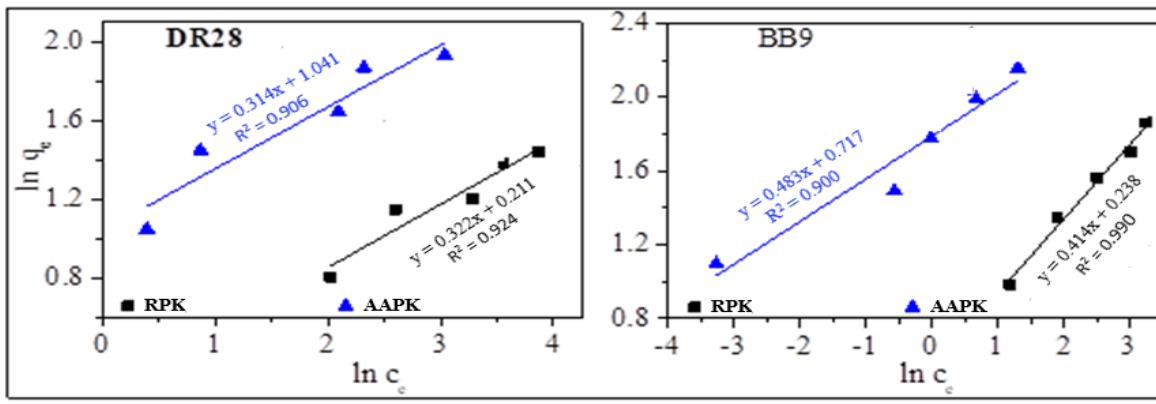

(b)

Figure 6: (a) Langmuir adsorption isotherms **(b)** Freundlich adsorption isotherms for the two dyes.

DISCUSSION

Characteristics of the raw and the acid-activated clays

The results from the characterization of the raw and the treated clays offer valuable insights into the structural, mineralogical, chemical, and physical transformations that take place in the kaolin clay during the acid activation process. These transformations have broad implications for the clay's utility in adsorption applications, particularly in the context of dye removal, as exemplified by BB9 and DR28.

The ATR-FTIR analysis of both the raw kaolin (RPK) and the acid-activated kaolin (AAPK) provided critical insights into their functional groups. The observed significant differences in absorption bands between the two clays proposed the presence of amorphous silica (Boukhemkhem and Rida, 2017). Such observation is in good agreement with findings from other researchers (Gao et al., 2016). The acid activation process induced structural changes within the clay. The transformation of crystalline kaolinite into a more amorphous structure in AAPK, accompanied by the presence of amorphous silica, highlights the efficacy of acid treatment in modifying the clay's composition. It implies that acid activation effectively disrupts the crystalline nature of kaolinite in RPK, making it more open to adsorption, a conclusion supported by earlier research (Nayak and Singh, 2007). A comparison of the ATR-FTIR spectra before and after adsorption revealed that BB9 adsorption resulted in a more ordered kaolinite than DR28, which is in fairly good agreement with the observed entropy values obtained in this study. The observation is closely related to

the ones reported by other researchers (Monash et al., 2011).

The XRD analysis confirmed and expanded upon the changes observed in the functional groups. By revealing the disappearance of kaolinite peaks in AAPK and the presence of tridymite, it demonstrates how high-temperature calcination and the subsequent acid leaching impacted the raw kaolin. These processes result in the transformation of the material into a more amorphous metakaolin with heightened silica content. The shift from crystalline kaolinite to an amorphous structure aligns with the previous findings of impurity removal and the dissolution of structural Al^{3+} ions during acid leaching. Such structural changes are pivotal in enhancing the clay's capacity for adsorption (Boukhemkhem and Rida, 2017; Luo et al., 2017). The observed presence of microcline [KAlSi3O8] as an impurity in the clay sample is in good agreement with the previously reported findings (Lugwisha and Siafu, 2014; Lugwisha and Lunyungu, 2016), hence it can be inferred that the raw kaolin used in this study contained crystalline kaolinite with coarser grains. Microcline is a raw material that can decompose into kaolinite under proper conditions (Omang et al., 2019).

The presence of tridymite silica in the AAPK might be the result of calcination reaction of the kaolin clay at 750ºC, which accounts for increased silica content in the AAPK sample as it has been observed from XRF analysis in this study. Microcline and quartz maintained their prominent d values of 3.25 and 3.48 Å approximately to 32º and 30º 2θ, respectively, for microcline. For quartz, the d values were 3.35 and 4.20 Å approximately to 31º and 24.5º 2θ. Such observation implies that quartz and microcline were not affected by acid activation, similar to what was observed by other researchers (Luo et al. 2016). The calcination of kaolin at 750ºC probably accounts for the primary disappearance of kaolinite peaks resulting into the formation of a powderier amorphous metakaolin as a result of dihydroxylation (Luo et al., 2016). Acid leaching of the calcined kaolin accounts for further structural changes of raw kaolin due to dissolution of structural Al^{3+} ions, resulting into residue with increased silica content. Such finding is in good agreement with the finding reported by other researchers (Boukhemkhem and Rida, 2017; Luo et al., 2017). The finding also correlates well with the observed decreased percent composition of Al_2O_3 and the increased silica (SiO_2) content from the XRF analysis in this study.

The chemical compositions of the raw and the treated clays that were obtained from the XRF analysis revealed that the silica (SiO_2) and alumina (Al_2O_3) contents in the raw clay agreed with previous studies of the Pugu kaolin (Akwilapo and Wiik, 2004). After acid activation, six of the oxides i.e., SiO_2, CaO, K_2O, Na_2O, MnO, and P_2O_5 increased to varying degrees, while three of the oxides i.e., Al_2O_3, Fe_2O_3, and MgO decreased. These changes in the percentage compositions of the AAPK compared to the RPK suggested occurrences of structural and surface modification resulting in more exposure of the adsorptive sites, hence increasing its absorbance efficiency, as was also observed by Gao et al. (2016).

With regard to the physical characteristics, a comparison of the three physical parameters, i.e., surface area, pore volumes and pore diameters for the raw and acid-activated clays showed that the specific surface area of the raw clay was relatively low in a way that may render the adsorption efficiency of the raw clay to be low, supporting the necessity of its modification. The almost ten-fold increase of the surface area upon acid activation was significantly high to enable physical modification of the clay. Previous studies have indicated that the calcination of raw kaolin at temperatures above 150ºC has the potential to remove impurities including adsorbed water, which results in increased surface area and exposure of the adsorptive sites (Avila et al., 2021). Calcination of kaolin at a temperature of 750ºC employed in this study therefore removed the unwanted impurities and also transformed kaolin into porous amorphous metakaolin characterized by increased surface area. The formation of amorphous metakaolin was also supported by the XRD pattern, which indicated the disappearance of crystalline kaolinite in the

AAPK phases. Acid leaching of the calcined kaolin further removed any remained impurities that are acid soluble, resulting in further increased surface area. Concerning the pore volume, the aggregation of fine particles probably accounts for the decreased pore volume of the AAPK relative to the RPK. A similar observation was also reported by Monash et al. (2011) and Boukhemkhem and Rida (2017). The pore diameter of the AAPK increased almost nine-fold, which also indicates a significant modification to its properties. Collectively, these characteristics endorse acid activation as a promising avenue for the modification of kaolin clay, thereby rendering it more apt for adsorption applications. The increased surface area, the exposure of adsorptive sites, and the shift toward an amorphous structure in AAPK emphasize its efficacy as an adsorbent in comparison to RPK. It is worth noting that the suitability of clay as an adsorbent is closely tied to its physical and chemical attributes, and these characterizations emphasize the optimization of these attributes through the acid activation process.

Optimal conditions for maximizing adsorption efficiency

The obtained results additionally contributed valuable insights into the optimal conditions for maximizing adsorption efficiency. These conditions encompass the choice of sulfuric acid concentration, as well as several parameters, including the impact of temperature, the influence of adsorbent dose, the role of initial pH, and the interaction with contact time and initial concentration. Understanding these factors is useful in enabling the fine-tuning of adsorption processes to ensure optimal removal of dyes like BB9 and DR28.

The results of this study show that the effect of temperature on the adsorption of the two dyes agrees with the thermochemistry concept that an exothermic process usually become more favorable as temperature decreases, which is vice-versa for an endothermic reaction. The variation in adsorption efficiency was proportional to the surface area of the adsorbents. These results are comparable to others previously reported in the literature (Sejie and Nadiye-Tabbiruka, 2016).

Concerning the effect of the adsorbent dose on the adsorption of the two dyes, this accounts for increased adsorptive sites and surface area hence increased adsorption efficiency as well. In general, kaolin clay possesses a negative structural charge hence a strong affinity to the cationic adsorbates compared to an anionic adsorbate. The second reason might be the molecular size of the adsorbates. BB9 has a smaller molecule size and hence exerts weaker intra-repulsion force per unit adsorptive sites while DR28 is likely to exert stronger intra-repulsion forces per unit adsorptive site. Another possible explanation for the observed trends is the assumption that every adsorbent molecule is saturated with adsorbate molecules at equilibrium. For low adsorbent dose, this assumption was approximately obeyed while for higher doses adsorbent molecules were not saturated with adsorbate molecules. As a result, the adsorption capacity for a higher adsorbent dose becomes smaller compared to the lower adsorbent dose. Such variations were also observed by Nandi et al. (2009).

The role of pH was such that, a higher pH increased the dye adsorption, particularly for the BB9. This was due to the increased electrostatic interaction between the cationic dye BB9 and the adsorbents, arising from the increased strength of negative charge on respective adsorbents as pH increased (Nandi et al., 2009). At the pH of 5 which is less than the pH_{ZPC} (6.04), the adsorbents developed more surface positive charge accounting for observed optimal adsorption. However, at a much lower pH than 5, there are probably stronger competitions for developed positive surface charge resulting in repulsion between the relatively large molecules of DR28 adsorbates. The effect of such repulsion accounts for the observed decreased adsorption efficiency. Furthermore, at pH greater than the pH_{ZPC} adsorbents began to develop negative charge hence account for decreased adsorption as pH increased due to repulsion between negative surface charge and charge of the anionic DR28 adsorbate (Olaremu, 2015). Similar observations of the adsorption

behavior of kaolin as a function of pH have also been reported by other researchers (e.g., Lugwisha and Lunyungu, 2016).

Observations from the variation of the and initial concentration with the adsorption efficiency showed that the percentage of color removal decreased with increased initial adsorbate concentration. The observation can be explained in terms of available surface area relative to the number of adsorbate molecules available. For the adsorption system with an initial higher concentration; the available adsorbent surface area as well as adsorptive sites are not enough to adsorb available large number of adsorbate molecules to a greater extent compared to the adsorption system with an initial lower adsorbate concentration. As a result, the adsorption system with an initial higher concentration exhibited a higher equilibrium concentration than a system with an initial lower concentration; thus, accounting for the observed decreased color removal with increased initial adsorbate concentration. This suggests that more contact time and adsorbent dose are required under the condition of an initial high concentration of adsorbates for effective color removal, similar to what was observed by Sejie and Nadiye-Tabbiruka (2016). In general, both RPK and AAPK adsorbents indicated a similar trend of the adsorption efficiency against BB9 and DR28 adsorbates. BB9 was adsorbed more than DR28 for both adsorbents, which is likely due to the fact that kaolin naturally possesses a negative charge hence exhibiting a strong affinity against cationic adsorbates compared to anionic adsorbates (Kumar et al., 2013).

The results from the adsorption isotherms show revealed that the activated kaolin showed better adsorption than the raw kaolin due to the respective higher values of adsorption intensity. Comparable findings have been reported by Boukhemkhem and Rida (2017) and Patabandige et al. (2019). The BBP adsorbent system displayed lower values of Gibb's free energy at various temperature ranges than the DR28 adsorption system, implying that the respective adsorption process was more feasible and spontaneous for the BB9 system. This likely also accounts for higher adsorption of BB9 than DR28.

Conclusion

In this study, we explored the outcomes and optimal conditions for treating Pugu kaolin, a local clay from Tanzania, to enhance its efficiency in absorbing synthetic dyes from water. We utilized the adsorption technique under varying conditions, using BB9 and DR28 as representative water-soluble dyes. Characterization of the clay through ATR-FTIR, XRD, and XRF showed that the raw clay exhibited absorption bands indicative of crystalline kaolinite with physisorbed water [$Al_2Si_2O_5(OH)_4$], silica [SiO_2], and microcline [$KAlSiO_3O_8$] phases. However, after acid activation the silica content increased while the alumina content decreased, due to the loss of the kaolinite phase. The modified kaolin clay, obtained through calcination at 750°C followed by acid activation using H_2SO_4 at various concentrations, exhibited significantly improved adsorption capacity for the removal of the two dyes, compared to the raw clay. This heightened adsorption capacity was attributed to an increased specific surface area and structural alterations that resulted from the removal of impurities. Optimal activation was achieved with H_2SO_4 at a concentration of 0.2 M, leading to adsorption efficiencies of 96.96% and 93.55% for BB9 and DR28 respectively.

The study also investigated the effects of various operating parameters that typically influence the adsorption efficiency, including temperature, contact time, initial pH of the adsorbate, initial concentration of the adsorbate, and adsorbent dose in the adsorption of the two dyes by both the raw and activated clays. It was revealed that under the conditions of 3 hours contact time 27°C temperature, 0.9 g adsorbent dose, initial pH of 11, and initial adsorbate concentration of 90 mg/L, the adsorption efficiency increased from 96.82% to 99.91% for BB9, and from 86.33% to 95.04% for DR28. While the raw kaolin clay exhibited somewhat weaker interactions with the adsorbates compared to its activated form, the efficiency obtained was still sufficiently reasonable, particularly for the BB9, to be used even without modification. These findings provide useful insights into the quality of the Pugu kaolin, as a low-cost, non-hazardous, and

efficient adsorbent in wastewater treatment and dye removal. Furthermore, it emphasizes the potential for further research in exploring additional particularities of the acid activation process, as well as the use of clay-based adsorbents in a broader spectrum of environmental remediation applications.

COMPETING INTERESTS

The authors declare that they have no competing interests.

AUTHORS' CONTRIBUTIONS

LE: Conceptualization, methodology, investigation, data curation. HHK: Writing of original draft, visualization. QAM: Conceptualization, methodology, supervision. EHJL: Conceptualization, methodology, supervision, mentorship.

ACKNOWLEDGEMENTS

The authors appreciate the contributions of technical staff at the Department of Geosciences, School of Mines and Geosciences, University of Dar es Salaam, and the African Minerals and Geosciences Centre, Kunduchi, Dar es Salaam in carrying out the instrumental analyses for this study.

REFERENCES

Akwilapo LD, Wiik K. 2004. Ceramic properties of pugu kaolin clays. Part 2: Effect of phase composition on flexural strength. *Bull. Chem. Soc. Ethiop.*, **18**: 1-10. DOI: https://doi.org/.4314/bcse.v18i1.61631

Aragaw TA, Angerasa FT. 2020. Synthesis and characterization of Ethiopian kaolin for the removal of basic yellow (BY 28) dye from aqueous solution as a potential adsorbent. *Heliyon*, **6**: e04975. DOI: https://doi.org/10.1016/j.heliyon.2020.e04975

Avila MC, Lick ID, Comelli NA, Ruiz ML. 2021. Adsorption of an anionic dye from aqueous solution on a treated clay. *Groundw. Sustain. Dev.*, **15**: 100688, DOI: https://doi.org/10.1016/j.gsd.2021.100688

Bentahar Y, Draoui K, Hurel C, Ajouyed O, Khairoun S, Marmier N. 2019. Physico-chemical characterization and valorization of swelling and non-swelling Moroccan clays in basic dye removal from aqueous solutions. *J. African Earth Sci.*, **154**: 80-88. DOI: https://doi.org/10.1016/j.jafrearsci.2019.03.017

Berradi M, Hsissou R, Khudhair M, Assouag M, Cherkaoui O, El Bachiri A, El Harfi A. 2019. Textile finishing dyes and their impact on aquatic environs. *Heliyon* **5**(11): e02711. DOI: https://doi.org/10.1016/j.heliyon.2019.e02711

Boukhemkhem A, Rida K. 2017. Improvement adsorption capacity of methylene blue onto modified tamazert kaolin. *Adsorpt. Sci. Technol.*, **35**(9-10): 1-21. DOI: https://doi.org/10.1177/0263617416684835

Caponi N, Collazzo GC, Jahn SL, Dotto GL, Mazutti MA, Foletto EL. 2017. Use of Brazilian kaolin as a potential low-cost adsorbent for the removal of malachite green from colored effluents. *Mater. Res.*, **20**: 2014-2022. DOI: https://doi.org/10.1590/1980-5373-MR-2016-0673

Chandan MR, Goyal S, Rizwan M, Imran M, Shaik AH. 2021. Removal of textile dye from synthetic wastewater using microporous polymer nanocomposite. *Bull. Mater. Sci.*, **44**: 272. DOI: https://doi.org/10.1007/s12034-021-02559-3

David MK, Okoro UC, Akpomie KG, Okey C, Oluwasola HO. 2020. Thermal and hydrothermal alkaline modification of kaolin for the adsorptive removal of lead(II) ions from aqueous solution. *SN Appl. Sci.*, **2**: 1134. DOI: https://doi.org/10.1007/s42452-020-2621-7

Gao W, Zhao S, Wu H, Deligeer W, Asuha S. 2016. Direct acid activation of kaolinite and its effects on the adsorption of methylene blue. *Appl. Clay Sci.* **126**: 98-106. DOI:

https://doi.org/10.1016/j.clay.2016.03.006

Gil A, Santamaría L, Korili SA, Vicente MA, Barbosa LV, de Souza SD. 2021. A review of organic-inorganic hybrid clay-based adsorbents for contaminants removal: Synthesis, perspectives and applications. *J. Environ. Chem. Eng.*, **9**: 105808. DOI: https://doi.org/10.1016/j.jece.2021.105808

He K, Zeng G, Chen A, Huang Z, Peng M, Huang T, Chen G. 2019. Graphene hybridized polydopamine-kaolin composite as effective adsorbent for methylene blue removal. *Compos. B. Eng.,* **161**: 141-149. DOI: https://doi.org/10.1016/j.compositesb.2018.10.063

Jawad AH, Abdulhameed AS. 2020. Facile synthesis of crosslinked chitosan-tripolyphosphate/kaolin clay composite for decolourization and COD reduction of remazol brilliant blue R dye: Optimization by using response surface methodology. *Colloids Surf. A. Physicochem. Eng. Asp.,* **605**: 125329. DOI: https://doi.org/10.1016/j.colsurfa.2020.125329

Kimambo V, Philip NYJ, Lugwisha E.H.J. 2014. Suitability of Tanzanian kaolin, quartz and feldspar as raw materials for the production of porcelain tiles. *Int. J. Sci. Technol. Soc.,* **2**: 201-209. DOI: https://doi.org/10.11648/j.ijsts.20140206.17

Kumar S, Panda AK, Singh R. 2013. Preparation and characterization of acid and alkaline treated kaolin clay. *Bull. Chem. React. Eng.,* **8**: 61-69. DOI: https://doi.org/10.9767/bcrec.8.1.4530.61-69

Li H, Wang H, Liu Q, Tan Y, Jiang N, Lin Y. 2016. Evaporation process for treating high-salinity industrial wastewater at low temperatures and ambient pressure. *Desalin. Water Treat.,* **57**(56): 27048-27060. DOI: http://dx.doi.org/10.1080/19443994.2016.1167126

Liu L, Luo X, Ding L, Luo S. 2019. Application of nanotechnology in the removal of heavy metal from water. In *Micro and Nano Technologies, Nanomaterials for the Removal of Pollutants and Resource Reutilization*, Luo X, Deng F (eds). Elsevier; 83-147. DOI: https://doi.org/10.1016/B978-0-12-814837-2.00004-4

Lugwisha EHJ, Lunyungu G. 2016. Water defluoridation capacity of Tanzanian kaolin-feldspar blend adsorbents. *Am. J. Appl. Chem*, **4**: 77-83. DOI: https://doi.org/10.11648/J.AJAC.20160403.12

Lugwisha EHJ, Siafu SI. 2014. The properties of feldspathic dental porcelain from Tanzanian aluminosilicate materials. *Int. J. Dev. Res.,* **4**: 2260-2265. URL: https://dspace.nm-aist.ac.tz/bitstream/handle/20.500.12479/197/JA_MEWES_2014.pdf?sequence=1&isAllowed=y

Luo J, Jiang T, Li G, Peng Z, Rao M, Zhang Y. 2017. Porous Materials from Thermally Activated Kaolinite: Preparation, Characterization and Application. *Materials*, **10**(6):647. DOI: https://doi.org/10.3390/ma10060647

Malima NM, Owonubi SJ, Lugwisha EHJ, Mwakaboko AS. 2021. Development of cost-effective and eco-friendly adsorbent by direct physical activation of Tanzanian Malangali kaolinite for efficient removal of heavy metals. *Mater. Today*: *Proc.,* **38**(2): 1126-1132. DOI: https://doi.org/10.1016/j.matpr.2020.06.469

Monash P, Niwas R, Pugazhenthi G. 2011. Utilization of ball clay adsorbents for the removal of crystal violet dye from aqueous solution. *Clean Technol. Environ. Policy,* **13**: 141-151. DOI: https://doi.org/10.1007/s10098-010-0292-6

Mudzielwana R, Gitaria MW, Ndungu P. 2019. Performance evaluation of surfactant modified kaolin clay in As(III) and As(V) adsorption from groundwater: adsorption kinetics, isotherms and thermodynamics. *Heliyon* **5**: e2756. DOI:

https://doi.org/10.1016/j.heliyon.2019.e02756

Mulushewa Z, Dinbore WT, Ayele Y. 2021. Removal of methylene blue from textile waste water using kaolin and zeolite-x synthesized from Ethiopian kaolin. *Environ. Anal. Health Toxicol.,* **36**(1): e2021007. DOI: https://doi.org/10.5620/eaht.2021007

Mustapha S, Ndamitso MM, Abdulkareem AS, Tijani JO, Mohammed AK, Shuaib DT. 2019. Potential of using kaolin as a natural adsorbent for the removal of pollutants from tannery wastewater. *Heliyon,* **5**(11): e02923. DOI: https://doi.org/10.1016/j.heliyon.2019.e02923

Nandi BK, Goswami A, Purkait MK. 2009. Adsorption characteristics of brilliant green dye on kaolin. *J. Hazard. Mater.*, **161**: 387-395. DOI: https://doi.org/10.1016/j.jhazmat.2008.03.110

Nayak PS, Singh B. 2007. Instrumental characterization of clay by XRF, XRD and FTIR. *Bull. Mater. Sci.,* **30**: 235-238. DOI: https://doi.org/10.1007/s12034-007-0042-5

Nwuzor IC, Chukwuneke JL, Nwanonenyi SC, Obasi HC, Ihekweme GO. 2018. Modification and physicochemical characterization of kaolin clay for adsorption of pollutants from industrial paint effluent. *Europ. J. Lipid Sci. Technol.,* **5**(8): 609-620.

Olaremu AG. 2015. Physico-chemical characterization of Akoko mined kaolin clay. *J. Minerals Mater. Charact. Eng.,* **3**: 353-361. DOI: https://doi.org/10.4236/jmmce.2015.35038

Omang B, Kudamnya EA, Owolabi AO, Odey J, Aniwetalu EU, Ako TA. 2019. Characterization of Kaolin deposits in Okpella and environs, Southern Nigeria. *Int. J. Geosci.,* **10**(3): 317-327. DOI: https://doi.org/10.4236/ijg.2019.103018

Patabandige DSBT, Wadumethrige SH, Wanniarachchi S. 2019. H_3PO_4-activated sawdust and rice husk as effective decolorizers for textile wastewater containing Reactive Black 5. *Int. J. Environ. Sci. Technol.,* **16**: 8375–8388. DOI: https://doi.org/10.1007/s13762-019-02394-4

Rahman A, Kishimoto N, Urabe T. 2015. Adsorption characteristics of clay adsorbents–sepiolite, kaolin and synthetic talc–for removal of reactive yellow 138. *Water Environ. J.,* **29**: 375-382. DOI: https://doi.org/10.1111/wej.12131

Sharma SK. 2015. *Green Chemistry for Dyes Removal from Waste Water: Research Trends and Applications*. John Wiley & Sons, Inc: Hoboken, New Jersey; P 496.

Sejie FP, Nadiye-Tabbiruka MS. 2016. Removal of Methyl Orange (MO) from water by adsorption onto modified local clay (Kaolinite). *Physical Chemistry,* **6**(2): 9-48. DOI: https://doi.org/10.5923/j.pc.20160602.02

Singh AK. 2016. Nanoparticle Ecotoxicology. In *Engineered Nanoparticles,* Singh AK (ed). Academic Press: Cambridge, Massachusetts; P 450. DOI: https://doi.org/10.1016/B978-0-12-801406-6.00008-X

UNEP (United Nations Environment Programme). 2021. Eastern Africa Atlas of Coastal Resources: Tanzania. URL: https://wedocs.unep.org/handle/20.500.11822/7515. Accessed November 21 2021.

Zaini NSM, Lenggoro IW, Naim MN, Yoshida N, Che Man H, AbuBakar NF, Puasa SW. 2021. Adsorptive capacity of spray-dried pH-treated bentonite and kaolin powders for ammonium removal. *Adv. Powder Technol.,* **32**(6): 1833-1843. DOI: https://doi.org/10.1016/j.apt.2021.02.036